Magnetic Resonance in Medicine 57:1148–1158 (2007)

Degenerate Mode Band-Pass Birdcage Coil for Accelerated Parallel Excitation

Vijayanand Alagappan,[1,2*] Juergen Nistler,[3] Elfar Adalsteinsson,[1,4,5] Kawin Setsompop,[5] Ulrich Fontius,[3] Adam Zelinski,[5] Markus Vester,[3] Graham C. Wiggins,[1] Franz Hebrank,[6] Wolfgang Renz,[3] Franz Schmitt,[3] and Lawrence L. Wald[1,4]

An eight-rung, 3T degenerate birdcage coil (DBC) was constructed and evaluated for accelerated parallel excitation of the head with eight independent excitation channels. Two mode configurations were tested. In the first, each of the eight loops formed by the birdcage was individually excited, producing an excitation pattern similar to a loop coil array. In the second configuration a Butler matrix transformed this "loop coil" basis set into a basis set representing the orthogonal modes of the birdcage coil. In this case the rung currents vary sinusoidally around the coil and only four of the eight modes have significant excitation capability (the other four produce anticircularly polarized (ACP) fields). The lowest useful mode produces the familiar uniform B_1 field pattern, and the higher-order modes produce center magnitude nulls and azimuthal phase variations. The measured magnitude and phase excitation profiles of the individual modes were used to generate one-, four-, six-, and eightfold-accelerated spatially tailored RF excitations with 2D and 3D *k*-space excitation trajectories. Transmit accelerations of up to six-fold were possible with acceptable levels of spatial artifact. The orthogonal basis set provided by the Butler matrix was found to be advantageous when an orthogonal subset of these modes was used to mitigate B_1 transmit inhomogeneities using parallel excitation. Magn Reson Med 57: 1148–1158, 2007. © 2007 Wiley-Liss, Inc.

Key words: transmit SENSE; array coils; tailored RF excitation; Butler Matrix; degenerate birdcage parallel excitation

The many positive benefits of high-field MRI are accompanied by destructive interference of the transmit RF fields within a typical volume excitation coil (1,2). This effect arises when the wavelength of the electromagnetic fields in the body approaches the dimension of the human head or body. In this case the RF fields generated by different parts of the coil can destructively interfere at some locations. For cylindrically symmetric coils, such as conventional birdcage designs, the center of the object is equidistant from all the rungs in the coil, which ensures an equal phase shift for the fields generated from each rung. For the phase relationship of the standard uniform mode of the birdcage, this leads to constructive interference at this location. In the periphery of the object, fields produced from different rungs travel unequal distances and can destructively interfere. The net effect is the center-brightening phenomena that is common in uniform mode birdcage coils at 3T and 7T. Although the high dielectric constant of water is, in practice, critical for shortening the wavelength, Collins et al. (2) have pointed out that the phenomenon does not require a dielectric media, and the phenomenon is not a dielectric resonance effect.

The B_1 excitation field inhomogeneity in the transmit coil leads to unwanted spatial variations in the tissue contrast and image intensity for most pulse sequences. The severity of the effect depends on the flip-angle dependence of the sequence, and since the problem arises during excitation, it is not easily dealt with in postprocessing. Where the intrinsic contrast information is not present locally, image manipulation cannot substitute for the missing information. A variety of methods have been explored to reduce the spatial variance in the B_1 excitation field. These methods include attempts to improve the high-frequency homogeneity of the RF coil (3) or to add local phase shifts to the RF wave with dielectric cushions (3) or detuned surface coils (4). Other methods have explored the theoretical potential of "RF shimming" (1,5,6). In these schemes, birdcage-like current elements are driven with tunable global phase and amplitudes that can deviate from the traditional uniform birdcage current distribution in order to improve the RF homogeneity across the sample.

A different approach alters the excitation scheme to reduce the flip-angle dependence of the contrast (7) or uses RF pulses with spatial profiles that approximately compensate for the transmit B_1 profile (8). Adiabatic RF pulses can mitigate the B_1 sensitivity of some excitations (9), although the highly nonlinear phase profile across the slice requires the application of additional techniques for many sequences.

2D and 3D spatially tailored excitation pulses can be designed to provide an arbitrary spatial pattern to the amplitude and phase of the transverse magnetization (10) subject to constraints on gradient and RF hardware. Thus, if the B_1 map of the excitation coil is known, a compensating excitation pattern can be designed that results in a uniform transverse magnetization after the excitation. While this is not the same as rendering the B_1 field uni-

[1]A.A. Martinos Center for Biomedical Imaging, Department of Radiology, Massachusetts General Hospital, Harvard Medical School, Charlestown, Massachusetts, USA.

[2]Department of Biomedical Engineering, Tufts University, Medford, Massachusetts, USA.

[3]Siemens Medical Solutions, Erlangen, Germany.

[4]Harvard-MIT Division of Health Sciences and Technology, Cambridge, Massachusetts, USA.

[5]Department of Electrical Engineering and Computer Science, MIT, Cambridge, Massachusetts, USA.

[6]Siemens Medical Solutions, Charlestown, Massachusetts, USA.

Grant sponsor: NCRR, National Institutes of Health; Grant number: P41RR14075; Grant sponsors: Siemens Medical Solutions; R.J. Shillman Career Development Award; MIND Institute.

*Correspondence to: Vijayanand Alagappan, A.A. Martinos Center, MGH, Bldg. 149, 13th Street, Rm. 2301, Charlestown, MA 02129. E-mail: vijay243@nmr.mgh.harvard.edu

Received 14 October 2006; revised 25 February 2007; accepted 27 February 2007.

DOI 10.1002/mrm.21247
Published online in Wiley InterScience (www.interscience.wiley.com).

form, it achieves the desired effect of making the flip-angle distribution and thus the image contrast uniform across the body similar to those produced by a uniform coil with a conventional excitation pulse.

Shaping the 2D or 3D spatial flip-angle distribution of an RF excitation in this way requires knowledge of the B_1 profile of the coils, as well as the application of a modulated RF amplitude and phase waveform while a gradient trajectory (usually a spiral or echo-planar trajectory (11)) is being played out. The principal practical limitation of this method is the length of time needed for the 2D or 3D excitation pulse. In a multichannel transmit coil, the differing spatial B_1 patterns of each coil can be used to accelerate the excitation *k*-space trajectory (12–14). In the accelerated parallel transmit case, a different time-dependent modulation of the RF phase and amplitude is sent to each channel. The principal goal is to reduce the length of the 2D and 3D spatial excitations and improve the off-resonance performance of the pulse. Thus, the spiral- or EPI-type gradient trajectory is accelerated R-fold compared to the Nyquist excitation sampling criteria in analogy to acceleration in parallel reception. The RF shimming method, with global phase and amplitude shifts to each coil and a conventional slice-selective excitation, can be viewed as a 1D, R = 1 parallel transmit excitation.

Similar to the receive array, the capability of the transmit array to accelerate the spatially shaped RF pulse depends on the spatially differing B_1 profiles of the array elements. While the ubiquity of MR systems with multiple receive channels has led to a great deal of effort in designing receive arrays, the lack of parallel transmit capability has led to less exploration of transmit coil geometries. Most transmit coil work has focused on "transceive arrays" for applications in which a uniform RF body coil is not available, and to potentially allow flexible excitation and reception in a single array, ultimately providing either B_1 shimming approaches or parallel transmit applications (15–18).

Most of the work toward developing multichannel transmit arrays has focused on the decoupled, lumped-element, strip-line array (18,19). The strip-line elements show a favorable lack of coupling when they are used in their original (nonlumped element) configuration and are closely shielded and trimmed to a $\lambda/4$ length (20). However, most studies have found it simpler to use the lumped-element approach and either have the elements far from one another (18) or decoupled with capacitive networks (17), or both (18). It is not possible to apply the direct analogy to preamplifier decoupling used for receive arrays in transmit since the power transfer requires a 50Ω impedance match for maximum power transfer. Nevertheless, a variety of methods have been proposed to decouple the transmit array coil. These methods include attempts to minimize the inductive coupling by overlapping the adjacent elements of an array (15), to control the currents in the coil using a current source instead of an voltage source (21), to use a Cartesian feedback approach (22), and to use a capacitive ladder network (23) to decouple the array coils.

In this work we developed a transmit array built of the modes of a degenerate birdcage coil (DBC) driven with and without a Butler matrix (24), and evaluated its performance for accelerated parallel transmit of spatially tailored 2D and 3D excitation pulses. An expected advantage of using the modes of a birdcage coil as excited by the Butler matrix is that they form naturally decoupled orthogonal modes that do not require decoupling strategies. The DBC utilizes the freedom to adjust the ratio of the rung and end-ring capacitors (C_{rung} and $-C_{ring}$) in a band-pass birdcage coil. Tropp showed (25) that as this ratio is adjusted, the coil makes a transition from high-pass to low-pass behavior, and at the transition point the modes of the coil are degenerate. A DBC built in this way has been utilized as a receive array (26) and a transmit array for RF shimming (27). Other methods have used coupling structures to selectively perturb the frequency of the gradient mode of a low-pass birdcage to be degenerate with the uniform mode to improve sensitivity (28) or to allow sensitivity encoding (SENSE) acceleration in reception (29). In addition, Cheng et al. (30) performed an elegant theoretical analysis of the mode structure of the DBC. Taracila et al. (31) used vector potential simulated patterns and considered how the magnitude images from the orthogonal modes of a DBC transmit-receive array could be combined to produce a uniform intensity image but not necessarily a uniform flip-angle excitation.

Beyond these investigations for reception, and theoretical investigations for transmission, to our knowledge the DBC has never been tested as a transmit array and only minimally as a receive array. With the exception of our preliminary work with the Butler matrix (32), the DBC has never been demonstrated with more than two of its orthogonal modes used for detection (as opposed to coupling into the loop-array basis set).

In our work we seek to use parallel excitation in conjunction with accelerated spatially tailored excitation pulses to produce 3D patterns of transverse magnetization following the excitation, including the uniform excitation pattern of constant flip angle across the object needed for uniform image contrast in many imaging sequences. In particular, we compare the two sets of modes (the loop-array basis set) and the orthogonal birdcage modes to assess the benefit of the extra flexibility in this design. Finally, the transmit validation is important because the phase variation of the modes is so critical for transmit, where, unlike reception, there is no "magnitude reconstruction" or opportunity to manipulate the loop-array mode data digitally to form the orthogonal modes.

MATERIALS AND METHODS

Eight-Channel Transmit System

The parallel excitation was performed on an eight-channel system consisting of a modified 3T Magnetom Trio, A Tim system (Siemens Medical Solutions, Erlangen, Germany) with gradient amplitude at 40 mT/m (G_x, G_y) and 45 mT/m (G_z), and slew rate at 200 mT/m/s. Eight sets of the RF waveform and gradient generation hardware were configured in a master and slave setup. A single master channel synchronized the waveforms of each of the seven slave transmit systems. Each subsystem was used to produce the independent phase and amplitude modulation needed for the independent transmit (TX) array channels, and in-

cluded B_0 eddy-current compensation, amplifier nonlinearity compensation, and specific absorption rate (SAR) monitoring. Each channel used a separate 8-kW RF amplifier (Dressler, Stolberg-Vicht, Germany). All of the experiments were performed on a 170-mm-diameter spherical phantom filled with low-dielectric synthetic oil (dimethylpolysiloxane (DMPS)). The spherical oil phantom was surrounded by a cylindrical loading ring to mimic the loading of the human head.

Sequence Parameters

The B_1 profile of each mode was inferred by reciprocity from a complex image acquired using the DBC mode for transmit and the RF body coil for reception. A low-flip-angle 3D gradient-recalled echo (GRE) sequence with $64 \times 64 \times 64$ pixels and $4 \times 4 \times 4$ mm resolution (TR/TE/BW = 20 ms/6 ms/400 Hz/pixel) was used. Both the 2D and 3D spatially tailored RF excitations were used in a conventional 3D GRE sequence (TR/TE = 30 ms/6 ms, matrix = $128 \times 128 \times 64$, in-plane resolution = 2 mm, partition thickness = 4 mm, and BW = 400 Hz/pixel).

Coil Construction

An eight-rung DBC (Fig. 1) was constructed on a 280-mm-diameter acrylic cylinder with 12-mm-wide conductors. The band-pass birdcage used a 200-mm rung length. The multiple resonant modes of the band-pass coil were collapsed to a single frequency by careful choice of the ratio of rung capacitances (C_{rung}) to the end-ring capacitance (C_{ring}). We estimated this ratio for the Larmor frequency based on a measurement made with only two of the eight loop segments of the birdcage present (Fig. 1). First, each loop was independently tuned via C_{rung} and C_{ring} to the Larmor frequency and matched to a 50Ω coaxial cable. Then the two loops were allowed to resonate simultaneously and the S_{12} coupling between them was measured. The value of the capacitor on the common rung was incrementally adjusted to improve the S_{12} decoupling. After each incremental adjustment of the common rung capacitor, one C_{ring} on each loop was adjusted to maintain the tuning of the loops. With the S_{12} isolation optimized, the three C_{rungs} were replaced with the optimum value found for the common rung and the coils were individually retuned with the appropriate C_{ring}. These values for C_{rung} and C_{ring} (18pF and 13pF) were used as initial values for all eight sections of the DBC.

Starting with the initial capacitance values, the birdcage coil was fine-tuned to degeneracy with only minor adjustments to C_{rung} and C_{ring} by adding additional rungs one at a time and checking the resonance frequency and S_{12} couplings of the added loop to the loops already constructed. Only one of the ring capacitors was perturbed to adjust the tuning of the loop. Finally, each loop section was coupled into a coaxial cable, and an RF cable trap was used to block common mode currents on the output coax. These traps were formed using five turns (~1 cm diameter) of semi-rigid coax bridged with a parallel capacitance tuned to create a resonant parallel LC circuit in the ground of the coax. An additional coaxial cable trap was placed 25 cm from the coil at the T/R switch for each channel.

B_1 Field Mapping

The RF body coil of the scanner was used for image reception in order to measure the magnitude and phase of the transmit B_1 profiles of the coil modes. The use of a separate and uniform reception coil simplified the measurement of the array's transmit field by simplifying the usual multiplicative modulation of the receive profile of the coil (we assumed the RF body coil was uniform over the FOV of the oil phantom.) For practical use, we anticipate that a dedicated receive-only array would be used for image reception, but for the purposes of evaluating the parallel transmit array, the use of a uniform body RF coil simplified the analysis of the excitation patterns. The use of a separate reception coil also allowed the relative phases of the transmit fields to be measured for simple GRE images. A separate reception coil is needed since a transceive coil image contains no information about phase of the transmit B_1 field. For the transceive case, the RF reception scales as B_1 and the excitation as B_1*; thus the detected image (the product of the two) loses all phase information (33). In order to allow the DBC array to be used as a "transmit-only" coil, each loop was detuned during receive by reverse biasing a series pin diode in each segment of the end-ring. Similarly, the body coil was dynamically detuned during the transmission with the local DBC. In the case of transmission with a mode of the DBC and reception with the spatially uniform body RF coil, the magnitude of the transmit B_1 field is proportional to the image intensity.

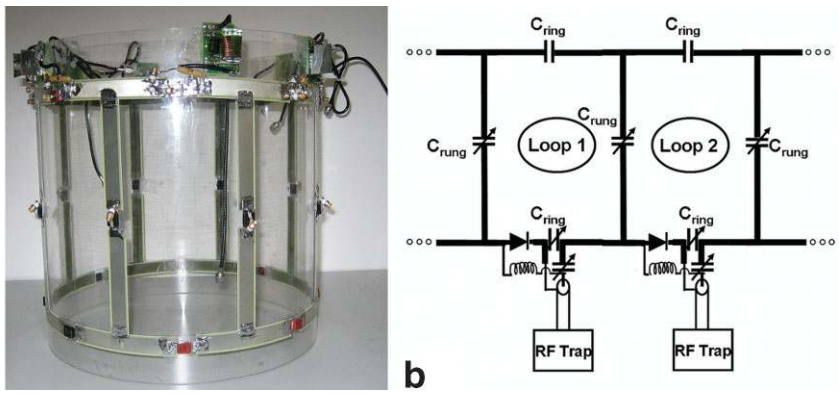

FIG. 1. Eight-rung DBC (**a**) and its schematic (**b**). The 280-mm-O.D. coil utilized 18pF capacitors in rungs and 13pF on the end-rings. Each drive port is fed across the end-ring capacitor and matched to 50Ω with a series capacitance. These coaxial driving cables were either independently excited with each transmit channel (loop-array mode configuration) or transformed by the Butler matrix into the birdcage mode configuration. [Color figure can be viewed in the online issue, which is available at www.interscience.wiley.com.]

The relative transmit B_1 phase was taken as the phase of the image received by the body RF coil. While this method assumes reception uniformity that may not be present in the body at high field, other quick, T_1-insensitive methods have been described (34). The absolute B_1 field at the center of the phantom was measured based on the double-flip-angle method (35), which utilizes the stimulated-echo concept by acquiring images with two flip angles α and 2α, where TR $\gg T_1$ (TR = 500 ms) such that the image signal is proportional to $\sin(\alpha)$ and $\sin(2\alpha)$, respectively. The B_1 field is derived from the ratio of signal magnitudes.

Butler Matrix and Birdcage Modes of the DBC

We evaluated the transmit DBC in the two different mode configurations. In the first configuration the RF power amplifiers directly feed the matched drive ports of each loop, as shown in Fig. 1. We refer to this configuration as the "loop coil" basis set because exciting a single port produces current only in the loop associated with that driving port. An 8 × 8 Butler matrix (24) was used to transform the "loop coil" basis set into the orthogonal mode configuration (36). The Butler matrix has eight coaxial inputs and eight coaxial outputs. It is constructed from 90° hybrids and phase shifters. The prototype eight-port, high-power, narrow-band Butler matrix schematic is shown in Fig. 2. The Butler matrix is the analog of a fast Fourier transform algorithm. It can also be thought of as a generalization of a quadrature hybrid. Like the quadrature hybrid in which a reflected wave is canceled if the mismatched load is symmetric, the Butler matrix has been found to provide reflection coefficients that are insensitive to the load (27).

A signal at any of the input ports produces equal amplitudes at all the output ports and a linear phase progression from port to port. The phase increment depends on which input port is used. The RF signal voltage (S_i) produced at output port i can be related to the amplitude and phase of the input waveforms (A_m and ϕ_m), where the subscript m corresponds to the mode (37):

$$S_i = \frac{1}{\sqrt{8}} \sum_m A_m e^{j\phi_m} e^{jm(i-1)\pi/4} \qquad [1]$$

If the RF waveform is incident only on input port $m = 1$, then the output ports generate rung currents with a sinusoidally varying phase from 0 to 2π as a function of rung number. Thus the $m = 1$ mode input generates the familiar circularly polarized (CP) uniform birdcage mode. A voltage waveform applied only on input port $m = -1$ generates the same field pattern with the opposite circular polarization (the antiquadrature excitation). An RF waveform incident only on input port $m = 2$ produces a similar sinusoidally varying phase relationship, but with twice the phase increment per rung. This is the first gradient mode of the birdcage coil. Similarly, RF voltage applied only on input port $m = -2$ produces the antiquadrature version of the $m = 2$ mode.

In principle, an eight-rung DBC driven by the Butler matrix can produce eight modes. The eight modes include three CP modes ($m = +1, +2, +3$); three anticircularly polarized (ACP) modes ($m = -1, -2, -3$); mode $m = 0$, which is the in-phase or coaxial mode with no phase variation between the rungs; and, finally, mode $m = 4$, the linear mode with a π phase shift between adjacent rungs. Based on the principle of reciprocity, which states that the field associated with reception has the opposite circular polarization of that associated with transmission, we label the CP modes as those CP modes with the correct circular polarization for efficient transmit, and the ACP modes as those correctly polarized for receive. The transmit CP modes ($m = +1, +2, +3$) and the receive ACP modes ($m = -1, -2, -3$) form two groups of orthogonal modes. Within each group the modes are orthogonal to each other in the sense that they have no mutual inductance, i.e., if U and V are the B_1 field vectors of each mode, then

$$\iiint \mathrm{U(x,y,z).V^*(x,y,z).dxdydz} = 0 \qquad [2]$$

Some combinations are also orthogonal between groups. Given two modes m and n from the eight choices (0, 1, 2, 3, 4,−1,−2,−3), then m is orthogonal to n if $|m| \neq |n|$. Thus, any two different modes from within the set of modes $m = +1, +2, +3$ (CP modes) are orthogonal to other modes within this set, as are any modes within the set $m = -1, -2, -3$ (ACP modes). Modes from the CP set will not be orthogonal to their equivalent in the ACP set (e.g., $m = +1$ is not orthogonal to $m = -1$), but note that $m = +1$ is orthogonal to $m = -2$.

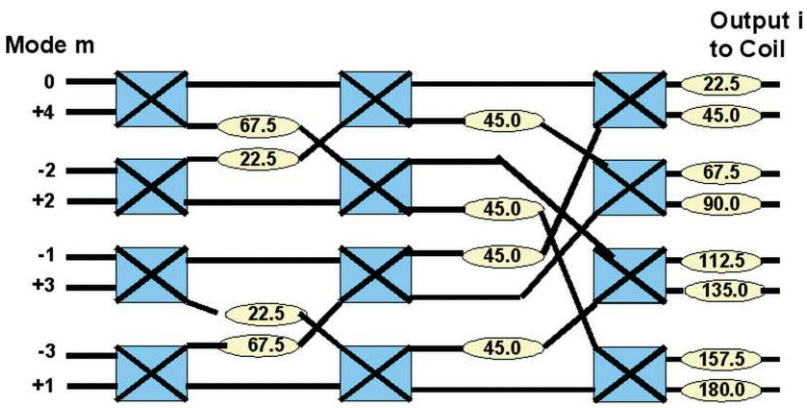

FIG. 2. Butler matrix schematic. The eight inputs and eight outputs are transformed by a network of 90° hybrids and phase shifters. The signal at the output port (S_i) can be calculated as the weighted sum of the input amplitudes and phases (A_m and ϕ_m). [Color figure can be viewed in the online issue, which is available at www.interscience.wiley.com.]

RF Pulse Design

We demonstrated the feasibility of the DBC for parallel excitation using accelerated 2D and 3D spatially selective excitations calculated from target excitation patterns and the measured B_1 field maps. Several methods have been proposed for the design of RF waveforms for parallel excitation in the low-flip-angle domain (12,13,38). We based our formulation on (14) the approach used by Grissom et al. (38). The small-tip multidimensional excitation approximation with N coils is written as

$$m(x) = j\gamma \sum_{n=1}^{N} S_n(x) \int B_{1,n}(t) e^{j.x \cdot k(t)} dt \qquad [3]$$

where S_n are the spatial excitation maps, $B_{1,n}$ are the RF waveforms for coils indexed by coil n, N is the total number of coils, x is the spatial variable, $m(x)$ is the desired target transverse magnetization after excitation, and $k(t)$ is the excitation k-space trajectory (defined as $k(t) = -\gamma \int_l^T G(\tau) d\tau$, where γ is the gyromagnetic ratio, G is the gradient, and T is the duration of the gradient waveform). After discretization of space and time, this expression can be written as a matrix equation $m = Ab$. The A-matrix incorporates the B_1 coil profiles modulated by the Fourier kernel due to the k-space traversal, and m is the target profile in space. These linear equations were solved for b, the sampled RF waveforms, by regularized pseudo-inverse via singular-value decomposition (SVD).

Two types of gradient trajectories were used (Fig. 3). The first trajectory consisted of a 2D excitation with a spiral trajectory in (k_x, k_y) and no transmit encoding in z. This was used to excite a high-resolution spatial pattern of letters (the MIT logo) in the (x,y)-plane. The resolution for the RF pulse design was set at 5 mm, FOV = 18 cm, and undersampled spiral trajectories were calculated for accelerations of integer factors of R = 4, 6, and 8 by successively increasing separation between the turns in the k-space trajectory. The spiral gradient waveform designs made use of routines made publicly available by Prof. B. Hargreaves, and operated with a gradient amplitude of 35 mT/m and a slew rate of 150 T/m/s (http://www-mrsrl.stanford.edu/~brian/vdspiral). The duration of the unaccelerated (R = 1) trajectory was 9.47 ms, and the durations for the R = 4, 6, and 8 trajectories were 2.42 ms, 1.64 ms, and 1.26 ms, respectively.

The second trajectory consisted of a 3D k-space excitation using a set of line segments or "spokes" in k_z, placed at regular intervals in the (k_x, k_y) plane (39). The spacing in the k_x, k_y plane corresponded to an FOV of 18 cm. The use of a sinc-like RF waveform during the transversal of each spoke achieves a sharp slice-selection in z, but with low-resolution control of the in-plane magnetization profile. This trajectory was used in conjunction with a uniform target magnetization profile to achieve a uniform excitation across the phantom despite the nonuniform nature of the excitation coils. Two versions of these trajectories were designed and tested: one with four spokes and one with one spoke at k_x, k_y = 0. For the four-spoke design the pulse length was 3.42 ms, and for the one-spoke design it was 1.2 ms.

RESULTS

Coil Decoupling and Field Maps

Tables 1 and 2 show the reflection measurement (S_{11}) and coil coupling (S_{12}) measures for the loop-coil basis set and the orthogonal birdcage basis set of the array, respectively. The average reflection measures were −20.47 dB for the loop coil basis set and −26.1 dB for the orthogonal birdcage basis. Thus, an additional benefit of the Butler matrix setup is the intrinsic matching to all RF power amplifiers in the presence of the load. Similarly to reflection cancellation at the transmit input of a quadrature combiner, the reflections at the mode ports of the Butler matrix are typically less than 10%, independently of the coil loading. This minimizes the power derating and gain variation of the amplifiers.

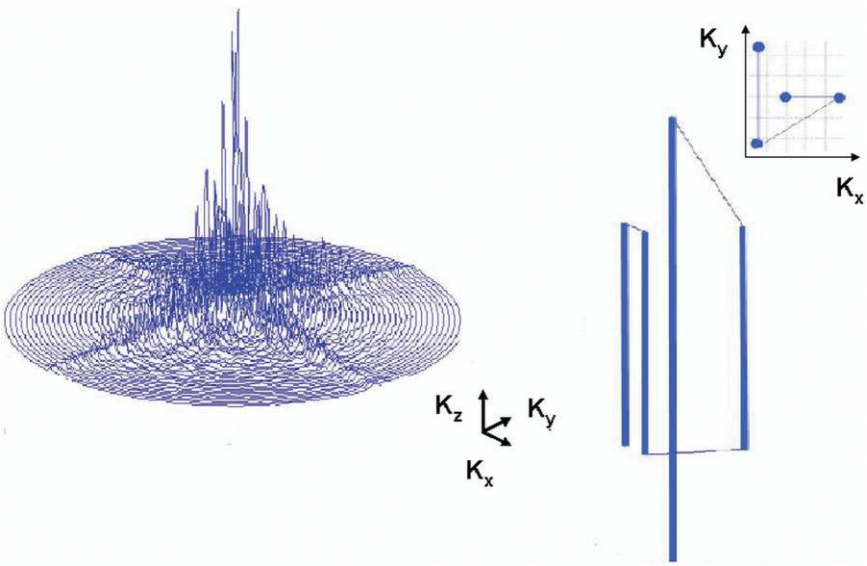

FIG. 3. **a:** The 2D spiral trajectory with the RF amplitude of a single RF channel overlaid. **b:** The 3D four-spoke trajectory. [Color figure can be viewed in the online issue, which is available at www.interscience.wiley.com.]

Table 1
S12 Coupling Between Elements of the Loop Coil Basis Set in dB*

Coil	S_{12} coil coupling of the loop coil basis set in dB							
	1	2	3	4	5	6	7	8
1	−20.5							
2	−16.9	−20						
3	−16.8	−17.9	−21.4					
4	−21.5	−18.3	−18.2	−20.2				
5	−28.9	−23.2	−16.6	−18.9	−20.5			
6	−21.3	−26.2	−21	−18.3	−18.5	−21.9		
7	−16.7	−19.3	−28.6	−21.6	−18.1	−18.7	−19.9	
8	−18.9	−18.3	−22.4	−27.5	−20.2	−16.1	−16.2	−19.4

*The diagonal elements represent the reflection measurement (S_{11}) in dB.

The CP and ACP modes of the Butler matrix provide load-independent matching to the RF power amplifier as long as the load is symmetric. The reflection measurements were done under two different load conditions: 1) a "light load" consisting of a 17-cm-diameter water sphere doped to a conductivity of 0.46 S/m (this phantom loads considerably less than the human head), and 2) a "head load" condition consisting of the same sphere filled with oil inside a heavily doped loading cylinder designed to mimic the head load. The average reflection measurement (S_{11}) for the eight-loop array modes were −7.92 dB under the light load conditions. The use of the Butler matrix improved this to −22.5 dB (average for all excluding the $m = 0$ and $m = 4$ modes, which are expected to have poor reflection measures.). For the "head load" condition, the reflection averages dropped from −21.5 dB (loop basis set average) to −30.55 dB (Butler matrix average excluding $m = 0, 4$). The exceptions are modes 0 and +4, which are linear modes and therefore their reflection factors are dependent on the loading of the array. Unlike the reflection measures, the isolation between the different modes is dependent on the loading condition.

The average decoupling between elements in the loop-coil basis set was −20.17 dB and the worst coupling was −16.1 dB. The average nearest-neighbor decoupling was −17.9 dB and the average next-nearest neighbor and higher-order neighbor decouplings were −17.36 dB and −22.4 dB, respectively. While the capacitive decoupling between nearest neighbors was explicitly optimized in the tuning procedure, we did not take any measures to adjust the decoupling between next-nearest neighbors. For the orthogonal birdcage modes, the CP modes are expected to couple to their partnering ACP modes. For example, if C_{mn} is the coupling between mode m and mode n, then $C_{-1,+1}$, $C_{-2,+2}$, $C_{-3,+3}$ are expected to couple. Excluding these three cases, the average coupling among the orthogonal birdcage modes was −34.8 dB.

The B_1 magnitude and phase profiles of the DBC are shown in Figs. 4 (loop array modes) and 5 (orthogonal birdcage modes). In both cases the field maps are in qualitative agreement with the expected patterns. The average B_1 field produced from each element at the center of the phantom was 2.605 μT for a 100V input to the 50Ω port. The ACP modes ($m = -1, -2, -3$) on average showed 4.3-fold lower signal than their corresponding CP modes ($m = 1, 2, 3$). For the normal mode ($m = 1$), the B_1 field in the center of the phantom was 4.269 μT for a 100V excitation.

Accelerated Parallel Excitation

Figure 6 shows GRE images from 2D spatially selective excitations accelerated at 1×, 4×, 6×, and 8× for both mode configurations. The B_1 pulse was appropriately scaled across the different accelerations to maintain an identical flip angle in the excited regions. The correlation between the simulated spatial profile and the experimentally obtained phantom image pattern was calculated to compare the two different coil configurations. The simulated spatial profile was obtained by performing a numerical Bloch equation simulation of the RF pulse for each pixel location within the phantom. The correlation coefficient between this simulated excitation and the measured image was calculated using MatLab (The Mathworks, Natick, MA, USA) as

Table 2
S12 Coupling Between Modes of the Orthogonal Birdcage Basis Set in dB*

Mode	S_{12} coil coupling of the orthogonal birdcage basis set in dB							
	−3	−2	−1	0	1	2	3	4
−3	−21.6							
−2	−46	−35.9						
−1	−28.9	−40	−28.6					
0	−29.9	−35.4	−27.7	−26.2				
1	−26.6	−34.9	−12.1	−31.7	−33.2			
2	−34	−11.5	−60	−24.6	−35.9	−25.5		
3	−13.1	−40.9	−26.4	−33.2	−33.6	−44.4	−27.3	
4	−27.5	−35.4	−50.5	−26.9	−38.4	−30.5	−27.3	−10.5

*The diagonal elements represent the reflection measurement (S_{11}) in dB.

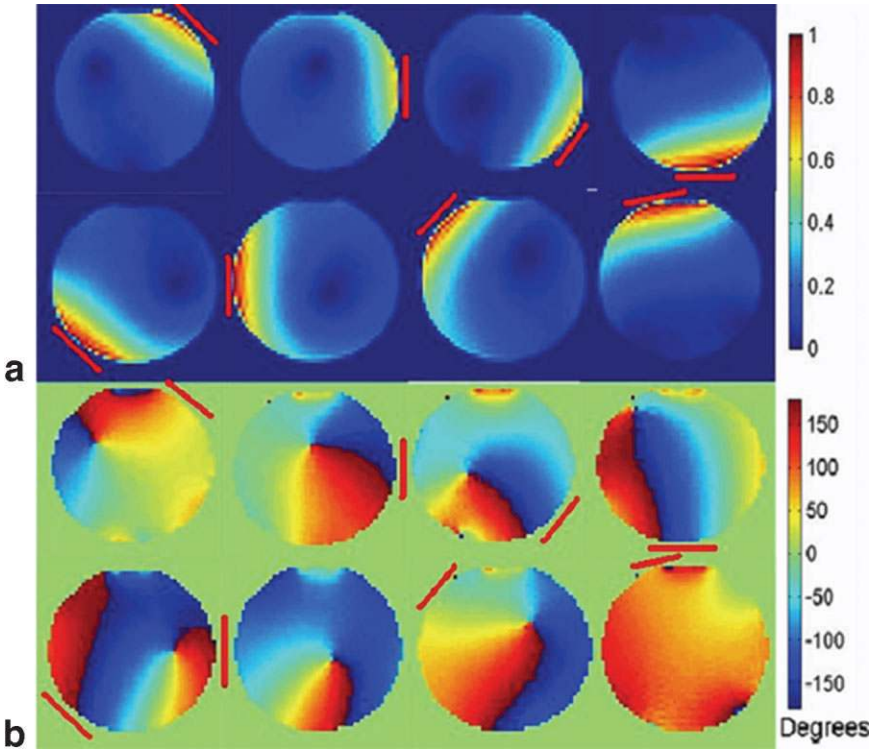

FIG. 4. (**a**) Magnitude and (**b**) phase profiles of the DBC in a loop array configuration. The red lines around the phantom indicate the position of the contributing loop within the DBC. The body coil was used for reception.

$$Corr = Cov(sim,data)/(\sigma sim.\sigma data) \quad [4]$$

where *Cov*(*sim*, *data*) is the covariance between simulation and data, calculated on magnitude maps within the phantom boundary, and σ is the standard deviation (SD) calculated over the same spatial domain. The correlation factor is shown in Table 3. At R = 1 and R = 4 accelerated excitations the correlation factors for the two basis sets were similar (~96%). The correlation factors did not significantly drop on acceleration (from R = 1 to R = 4). This may reflect the dominance of systematic errors in the B_1 map measurements over *g*-factor-like amplification of the transmit noise. An alternative possibility is that the improved robustness of the faster R = 4 trajectory to off-

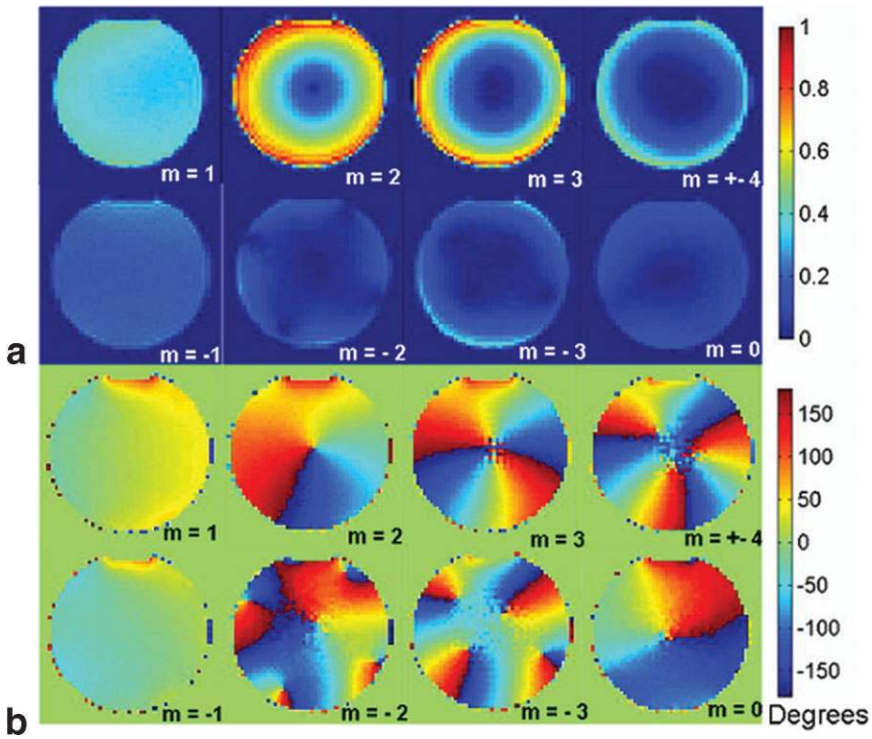

FIG. 5. (**a**) Magnitude and (**b**) phase profiles of the birdcage modes produced by the Butler matrix. The CP modes are the modes ($m = +1, +2, +3$) and the ACP modes are the modes ($m = -1, -2, -3$), mode $m = 0$ is the in-phase mode, and the phase $m = 4$ is the linear mode.

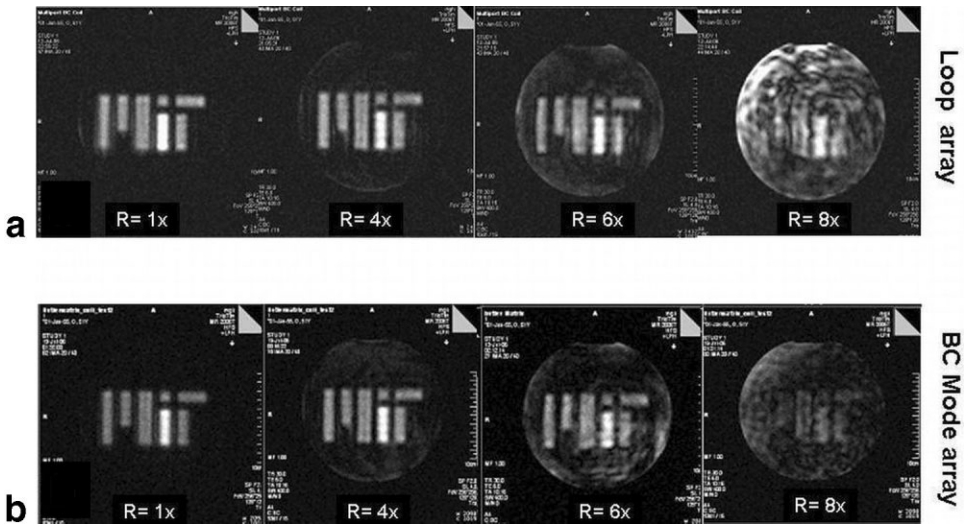

FIG. 6. 2D excitation profile with parallel transmission and acceleration R = 1, 4, 6, and 8. Pulse durations reduced from 9.47 ms for the 1× accelerated pulse to 2.42 ms for 4×, 1.64 ms for 6×, and 1.26 ms for 8× accelerated pulses. All of the pulses were calculated to produce identical flip angles within the excited region. **a:** Images from the DBC used in the loop-array configuration. **b:** Images from the orthogonal birdcage modes produced by the Butler matrix.

resonance effects compensated for increased *g*-factor artifacts. At R = 6 acceleration, the orthogonal birdcage basis set showed a higher artifact burden than the loop coil basis set (corr.factor = 87.50% and 92.57%, respectively).

Figure 7 shows the GRE images from the homogenous slice-selective excitation achieved with the one- and four-spoke 3D trajectory with a uniform target profile for both configurations of the DBC. The degree of homogeneity was compared by calculating the SD across the phantom as a percentage of the mean image intensity. Using only one spoke is equivalent to "RF shimming" of the slice-selective excitation.

The single-spoke homogeneity was found to be SD = 15.26% of the mean with the orthogonal basis set and SD = 16.48% of the mean with the loop coil basis set. For the four-spoke trajectory the corresponding homogeneities were 11.95% and 13.13%. The lower SDs for the four-spoke trajectory but similar results between the two mode sets suggest that increased gradient encoding is more useful than the choice of basis set for this application. The four-spoke loop coil basis set was observed to suffer from an image inhomogeneity near the air bubble in the phantom. This effect was not seen for the other configurations.

DISCUSSION

The orthogonal birdcage mode set was found to have good isolation, $C_{m,n}$, between pairs of modes m,n with the exception of $C_{-1,+1}$, $C_{-2,+2}$, and $C_{-3,+3}$. A first glance, it would appear these modes should be well isolated since the transmit and receive ports of a quadrature driven birdcage are known to be isolated. However, as Hoult (33) notes, it is important to keep the notation for the fields themselves separate from the terms proportional (by reciprocity) to transmission and reflection. For the uniform symmetric coil, the $m = 1$ field can be expressed as $U = (B_1\hat{x} + iB_1\hat{y})/2$, and the $m = -1$ field as $V = (B_1\hat{x} - iB_1\hat{y})^*/2$. In the case of a transmit array, it is only the efficiency of transmission that is relevant, and thus these two fields are appropriate as the product in the orthogonality condition. Then $U \cdot V^* = B_1^2$ is always positive and the integral cannot vanish, suggesting coupling between the $m = 1$ and -1 modes. In the case of the transmit receive birdcage, the reception process introduces a complex conjugate to the above expression for V and is proportional to $(B_1\hat{x} - iB_1\hat{y})/2$. In this case the dot product between U and V^* vanishes and we expect isolation between transmit and receive port of a quadrature birdcage driven by a hybrid coupler.

When an ideal DBC coil is driven in the ACP modes, no excitation is expected since the wrong sense of CP RF is generated (although in practice we did observe some excitation, presumably due to coupling to other modes and other imperfections in the coil.) Similarly, the coaxial mode ($m = 0$) should theoretically produce no excitation (since it lacks a current return path). Finally, while the capacitive decoupling between nearest neighbors was explicitly optimized in the tuning procedure, we did not take any measures to adjust the decoupling between next nearest neighbors. The theoretical work of Eagan et al. (40) suggests that it is not possible to decouple next-nearest neighbors using only two adjustable capacitors.

The CP and ACP modes were well matched to the RF amplifier independently of the load. However, for the linear mode $m = +4$ and the coaxial mode $m = 0$, the matching was poorer and dependent on the loading condition. For the $m = 0$ mode (rung currents in-phase), there is no return path for the current, and the coil should act like an open coax. For the $m = 4$ mode it is less clear, but the poor reflection properties of $m = 4$ were also found in Finite Difference Time Domain (FDTD) simulations (27),

Table 3
Correlation Factor in Percentage Between the Target Excitation Profile and the Obtained Experimental Excitation Profile for the 2D Spiral Trajectory MIT Logo

Acceleration	Loop coil basis set (%)	Orthogonal birdcage basis set (%)
1 x	96.05	96.44
4 x	95.70	95.84
6 x	92.57	87.50
8 x	53.51	57.22

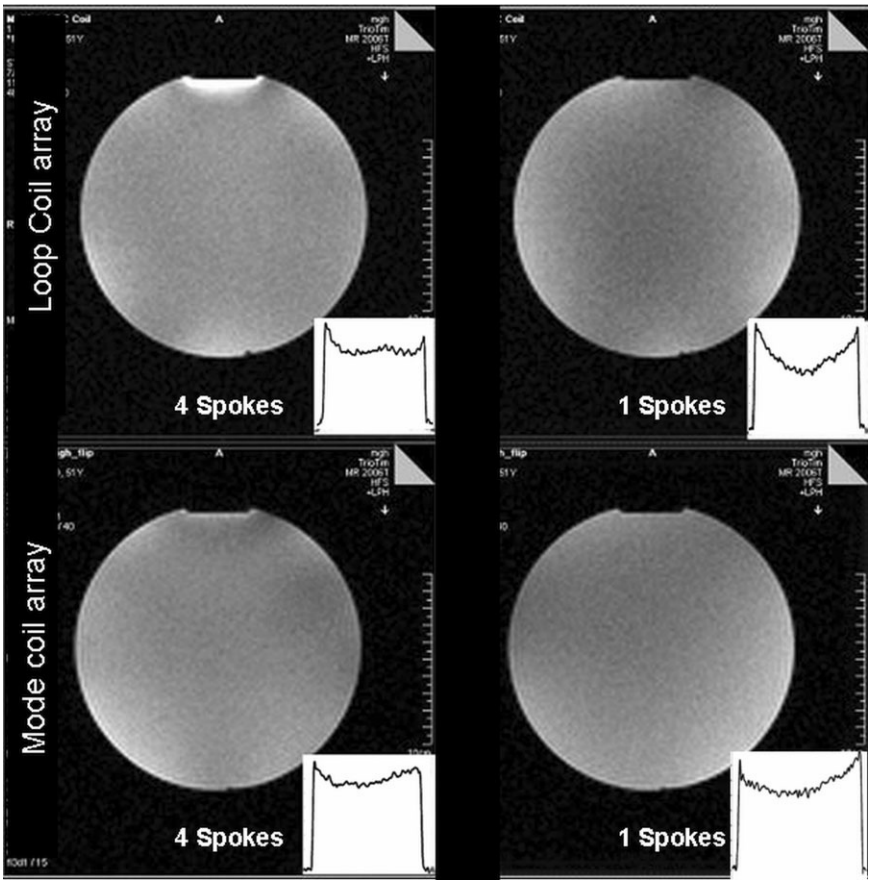

FIG. 7. Homogenous slice-selective excitation achieved with one (right) and four (left) spokes with the (**a**) loop coil basis set (top) and (**b**) orthogonal birdcage basis set (bottom). The indicated line profile through the center is shown in the bottom right corner of each image.

suggesting that this is not just an experimental imperfection.

Given that the same spatial information should be present in the two basis sets studied (loop coil modes and orthogonal birdcage modes), but half of the orthogonal birdcage modes are "dark" and in theory contribute little, we expect that the orthogonal birdcage mode choice should be significantly better for parallel imaging if only four independent transmit channels are available. This is an important consideration given the cost of additional transmit channels. To test this we generated an R = 4 accelerated trajectory using only every other mode of the loop coil basis set (similar field patterns to a gapped loop coil array) and compared it with an excitation formed from only the "bright" modes of the orthogonal birdcage set (three CP modes $m = +1, +2, +3$, and the linear mode $m = 4$). This comparison is shown in Fig. 8. The Butler matrix-driven orthogonal birdcage mode set was observed to have a significantly lower artifact burden when operated as a four-channel device. The correlation of the four loops and four "bright" modes with the target profile was 91.68% and 95.24%, respectively.

Figure 9 compares the R = 4 accelerated results from the reduced orthogonal birdcage mode ($m = 1, 2, 3, 4$; corr.fac-

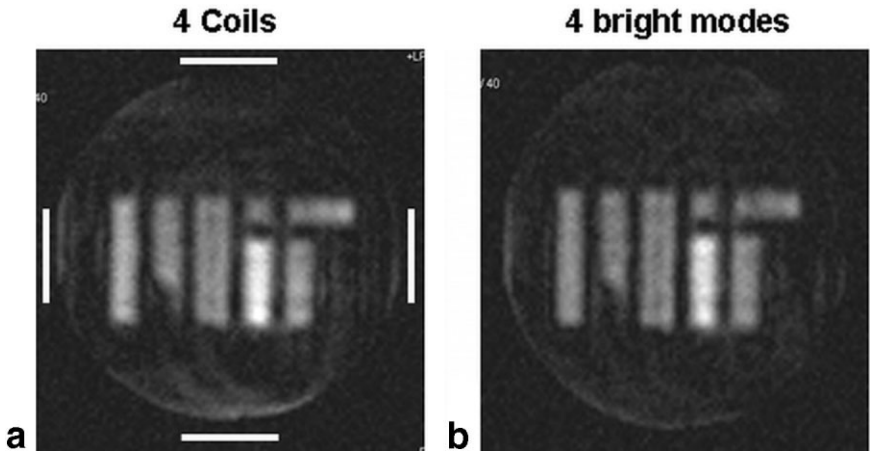

FIG. 8. R = 4 accelerated 2D excited GRE images obtained with (**a**) four alternate loops of the loop coil basis set (left) and (**b**) the "bright" modes of the orthogonal birdcage modes (right). The white lines indicate the position of the coils used for excitation in the loop coil basis set.

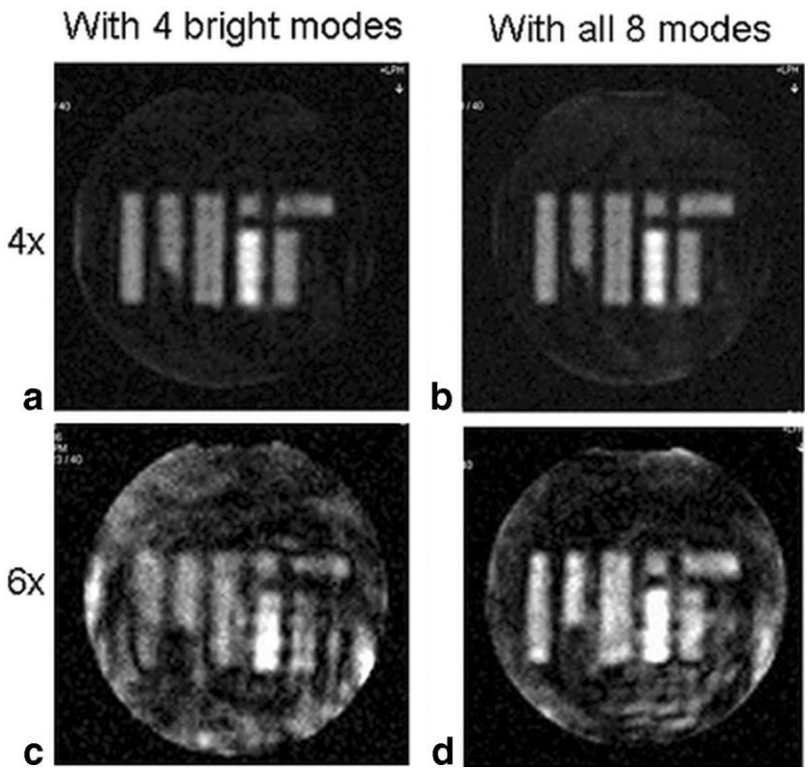

FIG. 9. Top row: R = 4 accelerated image from the orthogonal birdcage modes of the DBC. **a:** Using only the four "bright" modes (m = 1,2,3,4). **b:** Using all eight modes. Bottom row: R = 6 accelerated image from the orthogonal birdcage modes of the DBC. **c:** Using only the four "bright" modes (m = 1,2,3,4). **d:** Using all eight modes.

tor = 95.24%) with those obtained using all eight modes (corr.factor = 95.84%). There is very little difference, indicating that nearly all of the spatial information needed for the R = 4 accelerated pulse is contained in the four "bright" modes of the orthogonal birdcage basis set. Figure 9 (bottom row) compares the reduced "bright" mode set (corr.factor = 75.88 %) with the full set (corr.factor = 87.50 %) for R = 6. In this case the matrix inversion is underdetermined for the reduced mode set, yielding a poor excitation pattern, but apparently the "dark" modes add enough spatial information to reduce the ill-conditioning of the matrix central to the RF pulse design calculation.

CONCLUSIONS

We have demonstrated parallel transmit excitation using a transmit array based on the various modes of a degenerate mode birdcage coil. In addition to being a familiar structure used in most excitation coils, an array derived from a birdcage design allows flexibility in the choice of the modes used. In particular, we believe that the comparison of the two sets of modes (the loop-array basis set) and the birdcage modes gives this design an extra degree of flexibility and novelty. In addition to being naturally orthogonal, the birdcage modes have a convenient spatial B_1 pattern. The lowest mode is uniform in the long wavelength regime, and the higher-order modes have center magnitude nulls and thus complement the center brightening pattern that the uniform birdcage mode is seen to take on as the wavelength shortens. A comparison of the two basis sets for parallel transmission of a spatially tailored RF pulse showed that both basis sets performed approximately the same for this task, with the orthogonal birdcage modes performing better for accelerated transmit when only a subset of coils was used.

ACKNOWLEDGMENTS

We thank Professor Brian Hargreaves for making his spiral design routines available (http://www-mrsrl.stanford.edu/~brian/mritools.html).

REFERENCES

1. Hoult DI, Phil D. Sensitivity and power deposition in a high-field imaging experiment. J Magn Reson Imaging 2000;12:46–67.
2. Collins CM, Liu W, Schreiber W, Yang QX, Smith MB. Central brightening due to constructive interference with, without, and despite dielectric resonance. J Magn Reson Imaging 2005;21:192–196.
3. Alsop DC, Connick TJ, Mizsei G. A spiral volume coil for improved RF field homogeneity at high static magnetic field strength. Magn Reson Med 1998;40:49–54.
4. Schmitt M, Feiweier T, Voellmecke E, Lazar R, Krueger G, Reykowski A. B1-homogenization in abdominal imaging at 3T by means of coupling coils. In: Proceedings of the 13th Annual Meeting of ISMRM, Miami Beach, FL, USA, 2005 (Abstract 331).
5. Ibrahim TS, Lee R, Baertlein BA, Abduljalil AM, Zhu H, Robitaille PM. Effect of RF coil excitation on field inhomogeneity at ultra high fields: a field optimized TEM resonator. Magn Reson Imaging 2001;19:1339–1347.
6. Collins CM, Liu W, Swift BJ, Smith MB. Combination of optimized transmit arrays and some receive array reconstruction methods can yield homogeneous images at very high frequencies. Magn Reson Med 2005;54:1327–1332.
7. Thomas DL, De Vita E, Deichmann R, Turner R, Ordidge RJ. 3D MDEFT imaging of the human brain at 4.7 T with reduced sensitivity to radiofrequency inhomogeneity. Magn Reson Med 2005;53:1452–1458.
8. Deichmann R, Good CD, Turner R. RF inhomogeneity compensation in structural brain imaging. Magn Reson Med 2002;47:398–402.

9. Tannús A, Garwood M. Adiabatic pulses. NMR Biomed 1997;10:423–434.
10. Pauly J, Nishimura D, Macovski A. A k-space analysis of small-tip angle excitation. J Magn Reson 1989;81:43–56.
11. Stenger VA, Saekho S, Zhang Z, Yu S, Boada FE. B1 inhomogeneity reduction with transmit SENSE. In: Proceedings of the 2nd International Workshop on Parallel MRI, Zurich, Switzerland, 2004. p 94.
12. Zhu Y. Parallel excitation with an array of transmit coils. Magn Reson Med 2004;51:775–784.
13. Katscher U, Bornert P, Leussler C, van den Brink JS. Transmit SENSE. Magn Reson Med 2003;49:144–150.
14. Setsompop K, Wald LL, Alagappan V, Gagoski B, Hebrank F, Fontius F, Schmitt F, Adalsteinsson E. Parallel RF transmission with eight channels at 3 Tesla. Magn Reson Med 2006;56:1163–1171.
15. Alagappan V, Wiggins GC, Potthast A, Setsompop K, Adalsteinsoson E, Wald LL. An 8 channel transmit coil for transmit SENSE at 3T. In: Proceedings of the 14th Annual Meeting of ISMRM, Seattle, WA, USA, 2006 (Abstract 121).
16. Pinkerton RG, Barberi EA, Menon RS. Transceive surface coil array for magnetic resonance imaging of the human brain at 4 T. Magn Reson Med 2005;54:499–503.
17. Adriany G, Van de Moortele PF, Wiesinger F, Moeller S, Strupp JP, Andersen P, Snyder C, Zhang X, Chen W, Pruessmann KP, Boesiger P, Vaughan T, Ugurbil K. Transmit and receive transmission line arrays for 7 Tesla parallel imaging. Magn Reson Med 2005;53:434–445.
18. Lee RF, Hardy CJ, Sodickson DK, Bottomley PA. Lumped-element planar strip array (LPSA) for parallel MRI. Magn Reson Med 2004;51:172–183.
19. Adriany G, Van de Moortele P, Wiesinger F, Anderen P, Strupp JP, Zhang X, Snyder C, Chen W, Pruessmann KP, Boesiger P, Vaughan JT, Ugurbil K. Transceive stripline array for ultra high field parallel imaging applications. In: Proceedings of the 11th Annual Meeting of ISMRM, Toronto, Canada, 2003 (Abstract 474).
20. Lee RF, Westgate CR, Weiss RG, Newman DC, Bottomley PA. Planar strip array (PSA) for MRI. Magn Reson Med 2001;45:673–683.
21. Kurpad KN, Boskamp EB, Wright SM. Implementation of coil integrated RF power MOSFET as a voltage controlled current source in a transmit phased array coil. In: Proceedings of the 12th Annual Meeting of ISMRM, Kyoto, Japan, 2004 (Abstract 1585).
22. Hoult DI, Kolansky G, Kripiakevich D, King SB. The NMR multitransmit phased array: a Cartesian feedback approach. J Magn Reson 2004;171:64–70.
23. Jevtic J. Ladder networks for capacitive decoupling in phased array coils. In: Proceedings of the 9th Annual Meeting of ISMRM, Glasgow, Scotland, 2001 (Abstract 17).
24. Butler J, Lowe R. Beamforming matrix simplifies design of electronically scanned antennas. Electron Design 1961;9:170–173.
25. Tropp J. Mutual inductance in birdcage resonators. In: Proceedings of the 11th Annual Meeting of SMRM, Berlin, Germany, 1992. p 4009.
26. Leussler C, Stimma J, Roschmann P. The bandpass birdcage resonator modified as a coil array for simultaneous MR acquisition. In: Proceedings of the 5th Annual Meeting of ISMRM, Vancouver, Canada, 1997. p. 176.
27. Nistler J, Kurth R, Vester M, Renz W. B1 inhomogenisation using a multichannel transmit array. In: Proceedings of the 14th Annual Meeting of ISMRM, Seattle, WA, USA, 2006 (Abstract 2566).
28. Wong EC, Luh WM. A multimode, single frequency birdcage coil for high sensitivity multichannel whole volume imaging. In: Proceedings of the 7th Annual Meeting of ISMRM, Philadelphia, PA, USA, 1999. p. 165.
29. Lin FH, Kwong KK, Huang IJ, Belliveau JW, Wald LL. Degenerate mode birdcage volume coil for sensitivity-encoded imaging. Magn Reson Med 2003;50:1107–1111.
30. Cheng YC, Eagan TP, Chmielewski T, Flock J, Kang MC, Kidane TK, Shvartsman Sh M, Brown RW. A degeneracy study in the circulant and bordered-circulant approach to birdcage and planar coils. MAGMA 2003;16:103–111.
31. Taracila V, Petropoulos P, Eagan T, Brown R. Image uniformity improvement for birdcage like volume coils at 400 MHz using multichannel excitation. Concepts Magn Reson Part B 2006;29B:153–160.
32. Nistler J, Kurth R, Vester M, Renz W. B1 inhomogenisation using a multichannel transmit array. In: Proceedings of the 14th Annual Meeting of ISMRM, Seattle, WA, USA, 2006 (Abstract 2471).
33. Hoult DI. The principle of reciprocity in signal strength calculations—a mathematical guide. Concepts Magn Reson 2000;12:173–187.
34. Cunningham CH, Pauly JM, Nayak KS. Saturated double-angle method for rapid B1+ mapping. Magn Reson Med 2006;55:1326–1333.
35. Insko EK, Bolinger L. Mapping of the radiofrequency field. J Magn Reson Part A 1993;103:82–85.
36. Vester M, Nistler J, Oppelt R, Renz W. Using a mode concept to reduce the needs for multichannel transmit array. In: Proceedings of the 14th Annual Meeting of ISMRM, Seattle, WA, USA, 2006 (Abstract 2024).
37. Moody HJ. The systematic design of the Butler matrix. IEEE Trans Antenna Propag 1964:786–788.
38. Grissom W, Yip C-Y, Noll DC. A new method for the design of RF pulses in Transmit SENSE. In: Proceedings of the 2nd International Workshop on Parallel MRI, Zurich, Switzerland, 2004. p 95.
39. Ulloa J, Irarrazaval P, Hajnal JV. Exploring 3D RF shimming for slice selective imaging. In: Proceedings of the 13th Annual Meeting of ISMRM, Miami Beach, FL, USA, 2005 (Abstract 21).
40. Eagan TP, Cheng YCN, Kidane TK, Brown RW. A group theory approach to RF coil design. Concepts Magn Reson Part B Magn Reson Eng 2005;25B:42–52.